5. K.L. Wong and M.H. Chen, Single-feed small circular microstrip antenna with circular polarization, Microwave Opt Technol Lett 18 (1998), 394–397.
6. S.A. Bokhari, J.F. Zuercher, J.R. Mosig, and F.E. Gardiol,A small microstrip patch antenna with a convenient tuning option, IEEE Trans Antennas Propagat 44 (1996), 1521–1528.
7. W.S. Chen, C.K. Wu, and K.L. Wong, Compact circularly polarized circular microstrip antenna with cross slot and peripheral cuts, Electron Lett 34 (1998), 1040–1041.
8. K.L. Wong and Y.F. Lin, Circularly polarized microstrip antenna with a tuning stub, Electron Lett 34 (1998), 831–832.
9. K.L. Wong and M.H. Chen, Small slot-coupled small circularly polarized microstrip antenna with modified cross-slot and bent tuning-stub, Electron Lett 34 (1998), 1542–1543.
10. T.C. Yo, C.M. Lee, and C.H. Luo, Compact circular polarized patch antenna with harmonic rejection, Microwave Opt Technol Lett 50 (2008), 45–48.
11. P. Khotso, R. Lehmensiek, and R.R. van Zyl, Circularly polarized circular microstrip patch antenna loaded with four shorting posts for nanosatellite applications, Microwave Opt Technol Lett 54 (2012), 8–11.
12. O. Leonardi, M.G. Pavone, G. Sorbello, A.F. Morabito, and T. Isernia, Compact single-layer circularly polarized antenna for short-range communication systems, Microwave Opt Technol Lett 56 (2014), 1843–1846.

SMALL-SIZE NARROW OPEN-SLOT ANTENNA FOR THE 2.4/5.2/5.8-GHz WLAN OPERATION ALONG THE SIDE EDGE OF THE METAL-FRAMED SMARTPHONE

Kin-Lu Wong and Jun-Yu Lu
Department of Electrical Engineering, National Sun Yat-Sen University, Kaohsiung 80424, Taiwan; Corresponding author: wongkl@ema.ee.nsysu.edu.tw

Received 3 August 2015

ABSTRACT: *A small-size narrow open-slot antenna with 1-mm slot width and 12.7-mm slot length promising to be disposed in the narrow region along the side edge of the metal-framed smartphone for the 2.4/5.2/5.8-GHz WLAN operation is presented. This study exploits the narrow region between the display panel and the casing of the metal-framed smartphone to dispose the internal antenna therein. The proposed antenna is fed using a microstrip feedline with its tuning stub disposed within the slot, thereby keeping narrow width of the antenna. The open slot (denoted as a first slot) has a 1-mm opening disposed at the metal frame, and its length corresponds to only about 0.1 wavelength at 2450 MHz, which supports a fundamental open-slot mode to cover the 2.4 GHz band. In addition, with a chip capacitor (1.1 pF) loaded at a proper position across the first slot, the antenna can be reconfigured at about 5.2 GHz to create a new resonant open slot (second slot) from the capacitor to the slot opening. This second slot contributes to a new resonant mode for the antenna to cover the 5.2 GHz band. By embedding a series chip inductor (1.5 nH) in the microstrip feedline, a higher-order slot mode supported by the first slot can be shifted to cover the 5.8 GHz band. The antenna can hence cover the 2.4/5.2/5.8-GHz WLAN operation with a compact and narrow slot structure. Details of the proposed antenna are described.* © 2016 Wiley Periodicals, Inc. Microwave Opt Technol Lett 58:886–892, 2016; View this article online at wileyonlinelibrary.com. DOI 10.1002/mop.29698

Key words: *mobile antennas; WLAN antennas; metal-framed smartphone antennas; open-slot antennas; multiband antennas*

1. INTRODUCTION

The modern smartphone is generally with narrow regions along its side edges owing to the large display panel employed therein. The narrow regions greatly limit its availability for the internal antennas to fit in, mainly because the widths of many reported internal antennas are not of narrow widths (e.g., less than about 1 mm). In addition, for the modern smartphone with a slim profile, a metal frame is attractive to be added to increase the robustness of the device [1–7]. The appearance of such metal-framed smartphones is also attractive for many users. However, the presence of the metal frame can cause significant effects on the performance of the traditional internal antennas such as the inverted-F antennas or the shorted monopole antennas. For now, it is also noted that the internal antennas reported in the open literature that are suitable to be disposed in the narrow region along the side edges of the metal-framed smartphone are very scant. This motivates the present study.

In this article, we present a small-size narrow open-slot antenna promising to be disposed in the narrow region along the side edge of the metal-frame smartphone for the WLAN (wireless local area network) operation in the 2.4-GHz (2400–2484 MHz), 5.2-GHz (5150–5350 MHz), and 5.8-GHz (5725–5875 MHz) bands [8–11]. The antenna requires a short slot length of

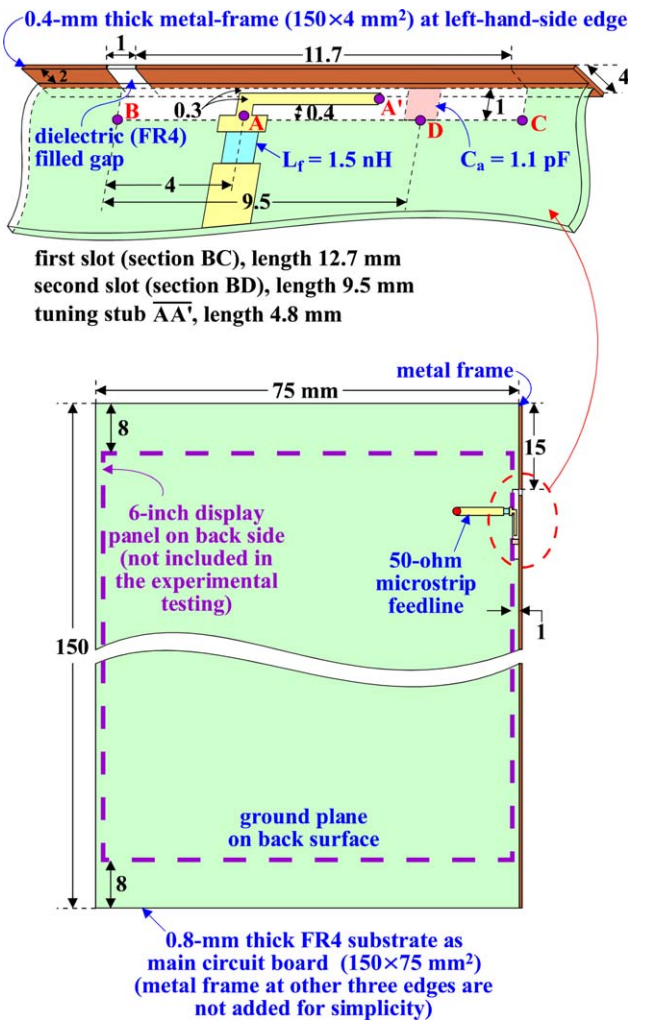

Figure 1 Geometry of the small-size narrow open-slot antenna for the 2.4/5.2/5.8-GHz WLAN operation along the side edge of the metal-framed smartphone. [Color figure can be viewed in the online issue, which is available at wileyonlinelibrary.com]

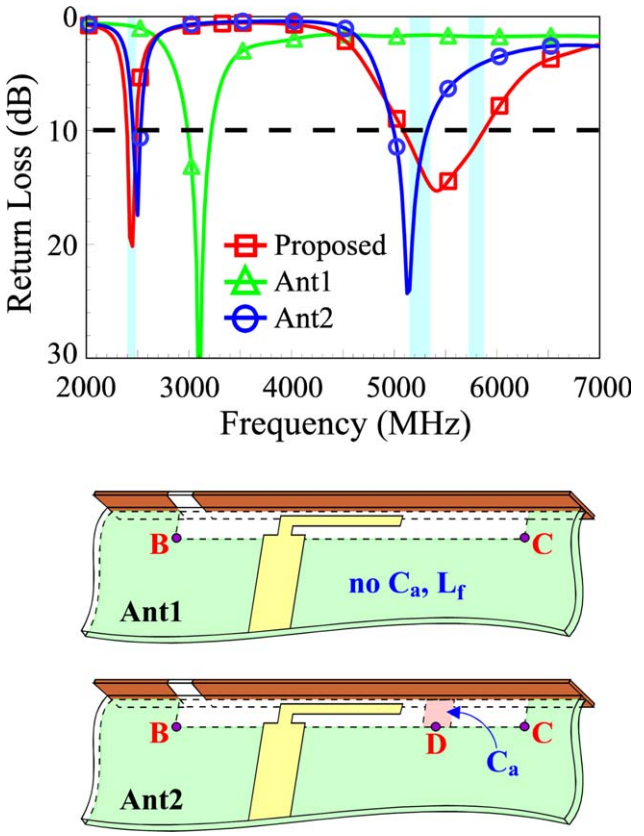

Figure 2 Simulated return loss for the proposed antenna, Ant1 (the case without C_a and L_f), and Ant2 (Ant1 with C_a). [Color figure can be viewed in the online issue, which is available at wileyonlinelibrary.com]

12.7 mm and has a narrow slot width of 1 mm only. The 1-mm narrow slot width makes the antenna promising to be disposed in the narrow region between the display panel and the metal frame of the smartphone. Note that the presence of the metal frame can lead to improved impedance matching of the open-slot antenna [6,7,12]. This attractive property makes the open-slot antenna very promising for applications in the metal-framed smartphone.

To achieve multiband operation for the small-size narrow open-slot antenna in this study, the techniques of loading a chip capacitor at a proper position across the narrow slot and embedding a series chip inductor in the microstrip feedline for the antenna are applied. The loading capacitor can exhibit relatively small reactive impedance at higher frequencies such as at frequencies higher than 5 GHz. In this case, the capacitor can behave like a short circuit, thereby creating a new resonant open slot from the capacitor to the slot opening disposed in the metal frame. This is equivalent to passively reconfiguring [13,14] the original open slot to create a new open slot therein to contribute an additional resonant mode for multiband operation. This additional resonant mode is adjusted to occur at about 5.2 GHz to cover the 5.2-GHz WLAN band. Since the reconfiguration of the antenna's open-slot resonant path is achieved by using a single capacitor, simple structure of the antenna can be retained. In addition, the capacitor can also cause the shifting of the antenna's fundamental open-slot mode to lower frequencies such as at about 2.4 GHz to cover the 2.4-GHz WLAN band. This effect also helps in decreasing the required size of the antenna.

Furthermore, the series inductor in the microstrip feedline can tune the antenna's higher-order slot mode to occur at about 5.8 GHz. Hence, with the capacitor loaded in the open slot and the series inductor embedded in the microstrip feedline, multiband operation for the antenna to cover the 2.4/5.2/5.8-GHz WLAN operation can be obtained. Details of the proposed antenna and its operating principle in achieving multiband WLAN operation are presented. Simulation and experimental results of the antenna are shown for discussion.

2. PROPOSED ANTENNA

2.1. Antenna Structure and Operating Principle

Figure 1 shows the proposed open-slot antenna for the 2.4/5.2/5.8-GHz WLAN operation in the metal-framed smartphone. As shown in the figure, the smartphone with a 6-inch display panel is studied. In this case, a 0.8-mm thick FR4 substrate of relative permittivity 4.4, loss tangent 0.02, and size 75 $\times\times$ 150 mm^2 is selected to be the main circuit board for the smartphone. On the back surface of the main circuit board, a ground plane is printed thereon. In addition, a 4-mm wide vertical metal frame is disposed along the right-hand-side edge of the main circuit board. The metal frame in the experimental study is formed by using a double-side grounded FR4 substrate of thickness 0.4 mm (see the photo shown in Fig. 9). The two ground planes on both sides are connected through adhesive copper foils at the edges to

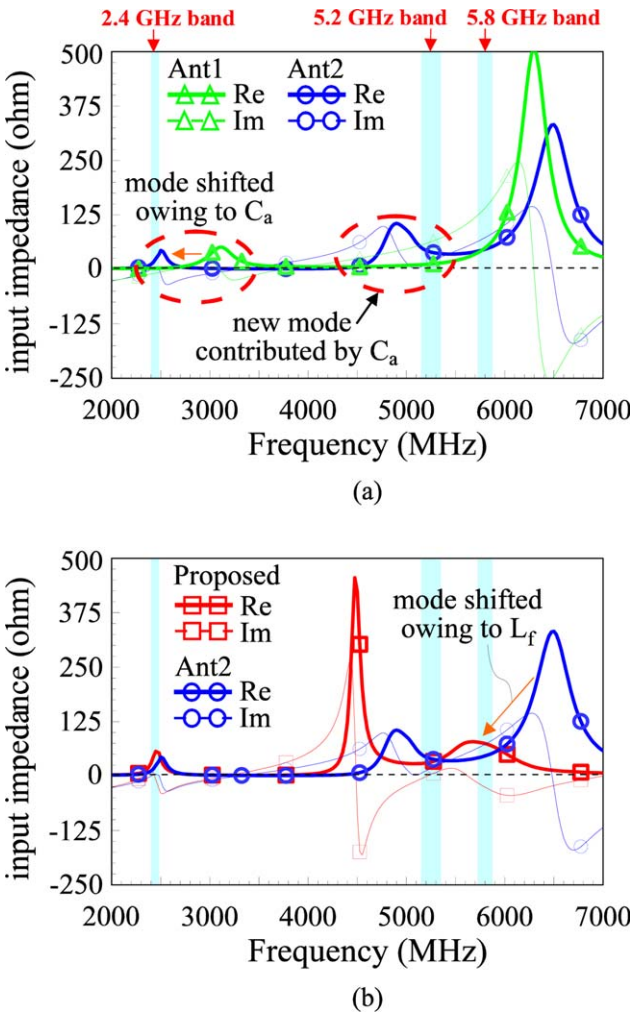

Figure 3 Simulated input impedance for (a) Ant1 and Ant2 and (b) Ant2 and the proposed antenna. [Color figure can be viewed in the online issue, which is available at wileyonlinelibrary.com]

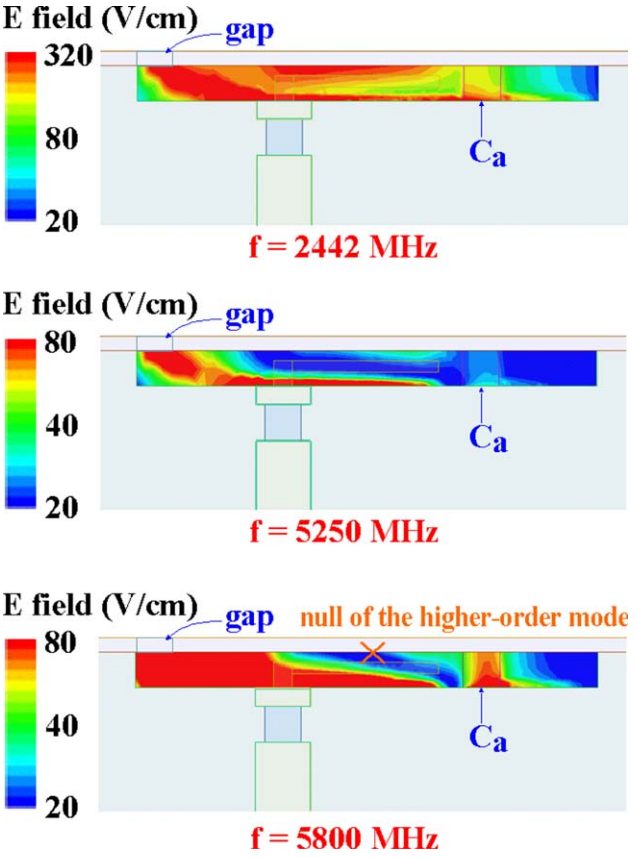

Figure 4 Simulated electric-field distribution at 2442, 5250, and 5800 MHz for the proposed antenna. [Color figure can be viewed in the online issue, which is available at wileyonlinelibrary.com]

simulate a 0.4-mm thick copper plate for the metal frame. There is also a no-ground gap of 1 mm on the metal frame, which serves as the opening of the open-slot antenna in this study. Note that for simplicity and without loss of generosity, the metal frame along the other three edges is not added.

It is noted that with the presence of the 6-inch display panel, the width of the region between the display panel and the metal frame is only 1 mm along the side edges of the main circuit board. To fit in such a narrow region, a narrow slot (section

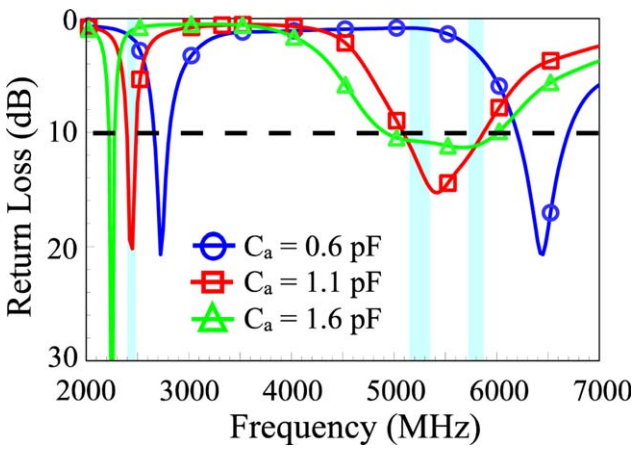

Figure 5 Simulated return loss as a function of the capacitor C_a across the slot for the proposed antenna. [Color figure can be viewed in the online issue, which is available at wileyonlinelibrary.com]

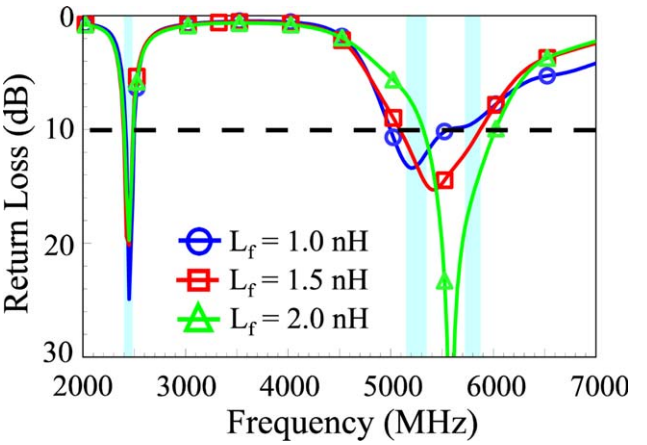

Figure 6 Simulated return loss as a function of the inductor L_f in the feedline for the proposed antenna. [Color figure can be viewed in the online issue, which is available at wileyonlinelibrary.com]

BC) of width 1 mm and length 12.7 mm is disposed therein, with one end of the narrow slot placed at the no-ground gap in the metal frame. With the proposed structure, a small-size narrow open-slot antenna is formed. The section BC is denoted as the first slot in this study.

To feed the narrow slot antenna, a 50-Ω microstrip feedline with a tuning stub (section AA′) of length 4.8 mm and width 0.3 mm is applied. Note that the section AA′ is disposed within the narrow slot, thereby keeping narrow width of the antenna. In order to achieve multiband operation for the 2.4/5.2/5.8-GHz WLAN operation, a chip capacitor of 1.1 pF (C_a) across the narrow slot is disposed at the position D and a series chip inductor of 1.1 nH (L_f) is embedded in the microstrip feedline. The capacitor C_a passively reconfigures the antenna to have a new resonant open slot (section BD, length 9.5 mm) to generate a new resonant mode at about 5.2 GHz for the 5.2-GHz WLAN operation. The new open slot is denoted as the second slot here.

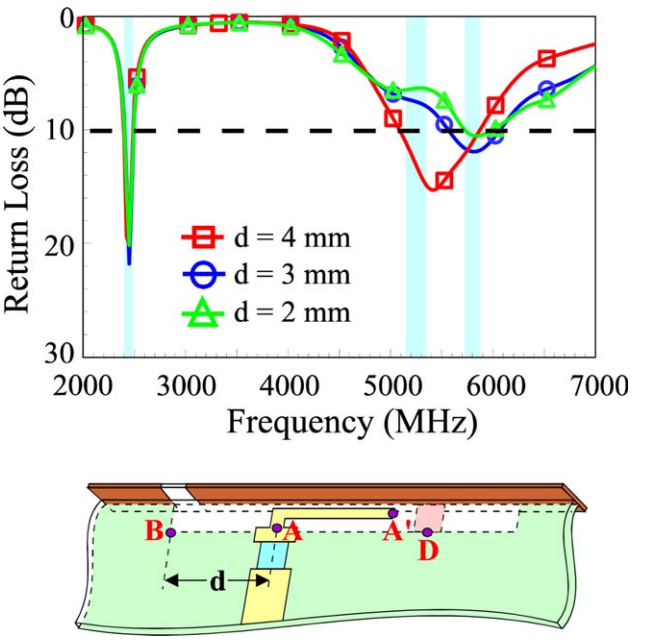

Figure 7 Simulated return loss as a function of the feedline position d for the proposed antenna. [Color figure can be viewed in the online issue, which is available at wileyonlinelibrary.com]

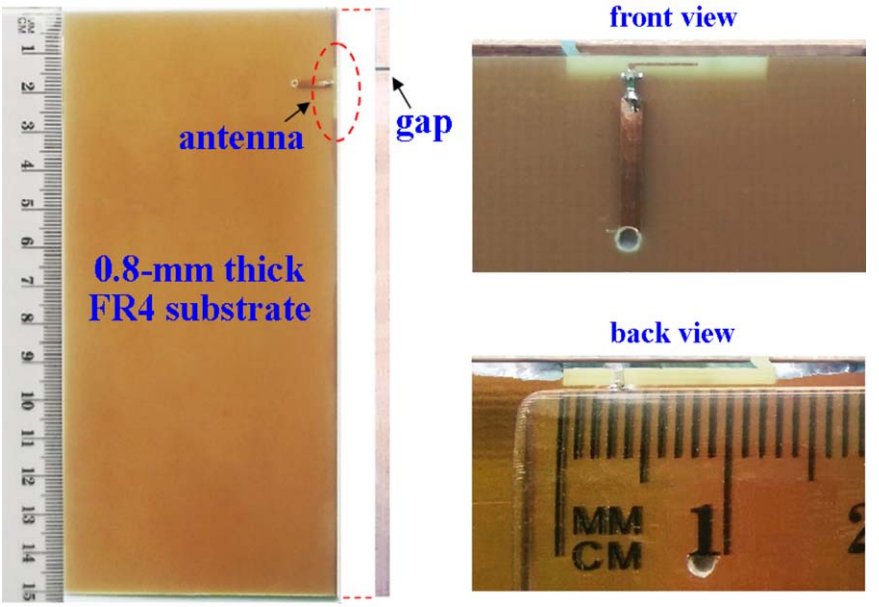

Figure 8 Photos of the fabricated antenna. [Color figure can be viewed in the online issue, which is available at wileyonlinelibrary.com]

The capacitor C_a can also shift the fundamental open-slot mode contributed by the first slot to lower frequencies, which helps in reducing the antenna size. Both the capacitor C_a and the substrate loading [7,15,16] on the first slot also decrease the required resonant length of the fundamental open-slot mode thereof. In this study, the length of the first slot is 12.7 mm only, which corresponds to about 0.1 wavelength at 2.4 GHz. The fundamental mode of the first slot can cover the 2.4-GHz WLAN operation. On the other hand, the inductor L_f can shift the higher-order mode of the first slot to occur at about 5.8 GHz, thus covering the 5.8-GHz WLAN operation.

To clearly describe the operating principle, Figure 2 shows the simulated return loss for the proposed antenna, Ant1 (the case without C_a and L_f), and Ant2 (Ant1 with C_a). For Ant1, there is only a resonant mode occurred at about 3.1 GHz, which is the fundamental open-slot mode contributed by the first slot (section BC). The three colored frequency regions in the figure represent the desired WLAN operation in the 2.4-GHz (2400–2484 MHz), 5.2-GHz (5150–5350 MHz), and-5.8 GHz (5725–

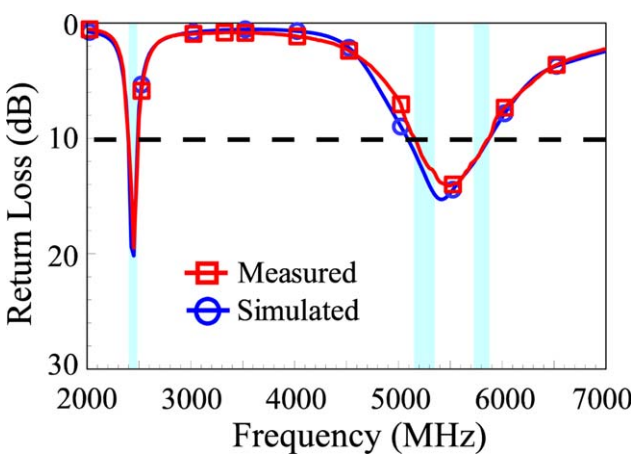

Figure 9 Measured and simulated return losses for the fabricated antenna. [Color figure can be viewed in the online issue, which is available at wileyonlinelibrary.com]

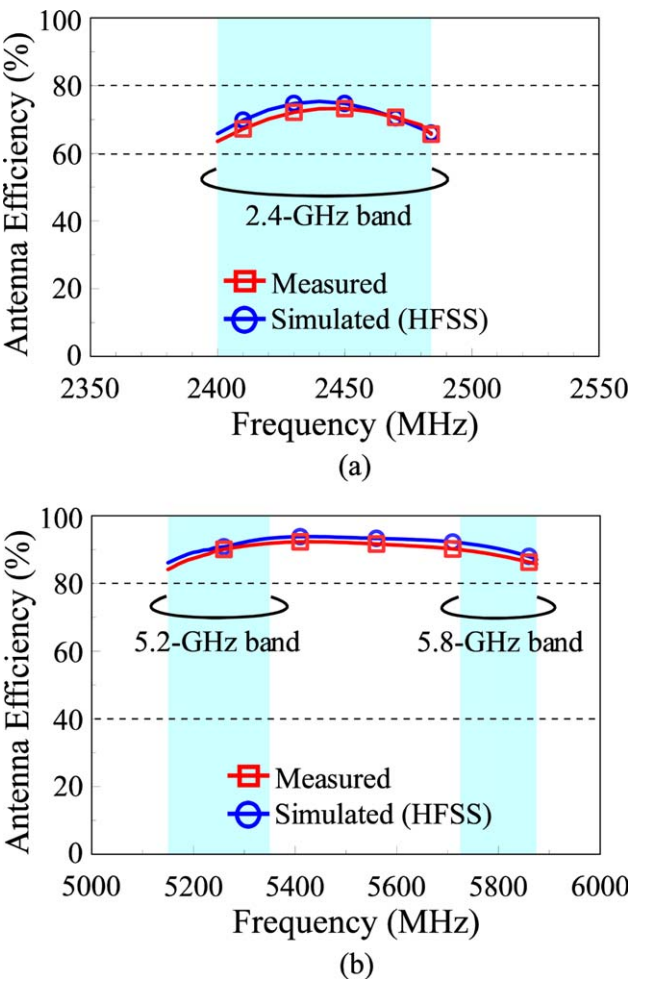

Figure 10 Measured and simulated antenna efficiencies for the fabricated antenna. (a) The 2.4-GHz WLAN band. (b) The 5.2/5.8-GHz WLAN bands. [Color figure can be viewed in the online issue, which is available at wileyonlinelibrary.com]

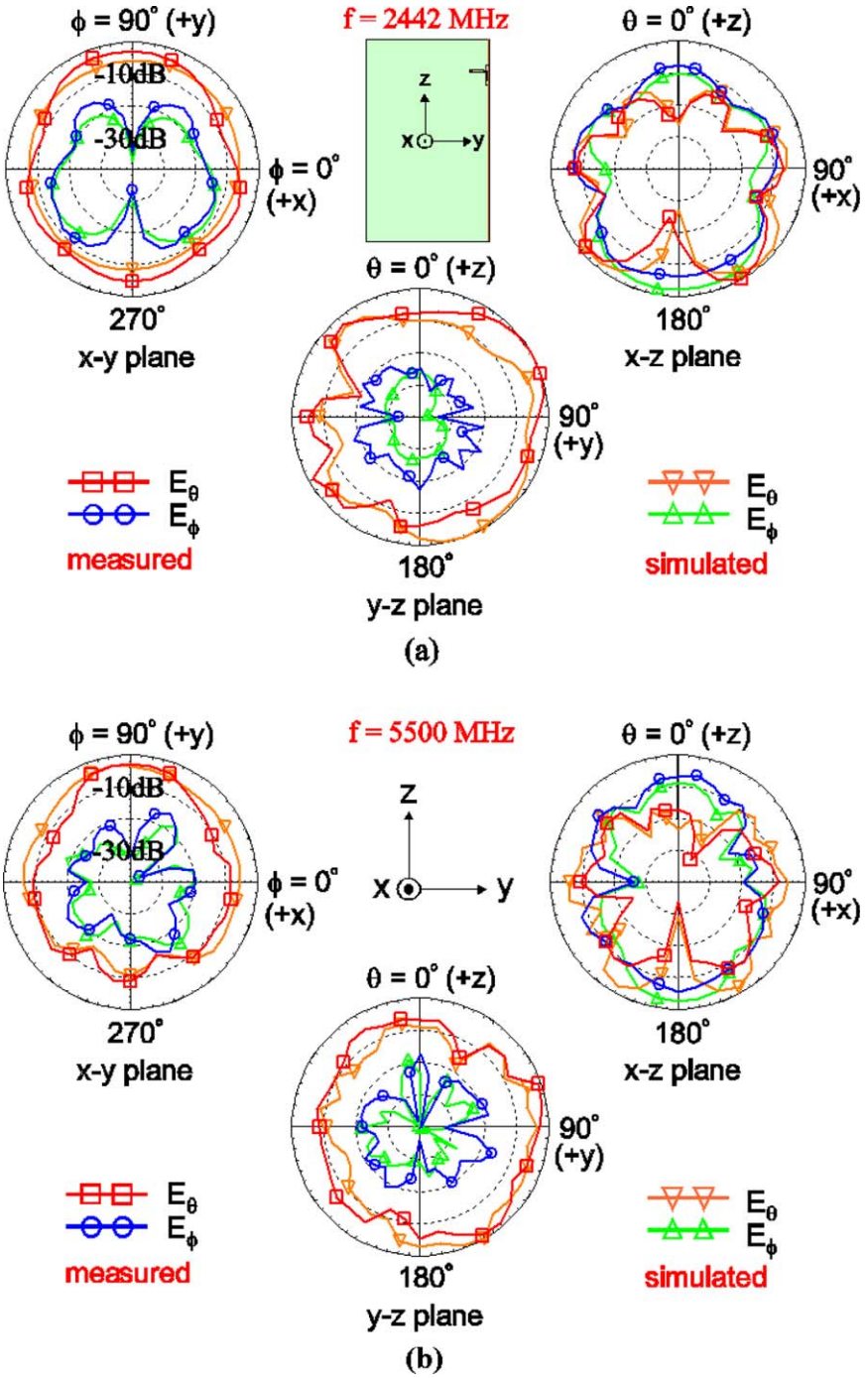

Figure 11 Measured and simulated radiation patterns for the fabricated antenna. [Color figure can be viewed in the online issue, which is available at wileyonlinelibrary.com]

5875 MHz) WLAN bands. With the capacitor C_a loaded at the position D across the narrow slot, the resonant mode at about 3.1 GHz is shifted to lower frequencies at about 2.4 GHz for the 2.4-GHz WLAN band (also see the simulated input impedance of Ant1 and Ant2 in Figure 3(a)). This frequency shifting is largely because the capacitor C_a intensifies the electric-field distribution in the first slot, thereby increasing the effective slot length and in turn decreasing the resonant frequency of the excited resonant mode accordingly. In addition, a new resonant mode occurring at about 5.2 GHz is seen for Ant2. This new mode generation is mainly contributed by the second slot, which is passively reconfigured [13] within the first slot owing to the capacitor functioning like a short circuit at higher frequencies. This new resonant mode can also be seen from the simulated input impedance shown in Figure 3(a).

For the proposed antenna, a wider bandwidth covering the 5.2-GHz and 5.8-GHz WLAN bands is obtained, which is owing to the series inductor L_f in the microstrip feedline. This wider bandwidth is obtained by the higher-order resonant mode of the first slot shifted from higher frequencies to about 5.8 GHz as shown in the simulated input impedance in Figure 3(b). This higher-order resonant mode combines with the one contributed by the second slot to achieve a wide bandwidth covering the 5.2-GHz and 5.8-GHz WLAN bands. It is also noted that the inductor L_f causes small effects on the antenna's low band at about 2.4 GHz. This property is advantageous, since it leads to

easy tuning of the proposed antenna to cover the multiband operation at 2.4, 5.2, and 5.8 GHz for the WLAN operation.

To further clarify the excited resonant modes for the proposed antenna, the simulated electric-field distributions at 2442, 5250, and 5800 MHz are presented in Figure 4. At 2442 MHz, strong electric fields are seen in the slot region near the 1-mm gap at the metal frame. The electric field in the slot region proximity to the capacitor C_a is also seen to be intensified, which can increase the effective resonant length of the first slot and decreases its corresponding resonant frequency. The electric-field distribution at 2442 MHz confirms that the resonant mode at about 2.4 GHz is mainly contributed by the first slot. At 5250 MHz, the excited electric-field distribution is seen to be confined in the second slot from the 1-mm gap to the capacitor. That is, the first slot is reconfigured to provide a new slot (second slot) therein, owing to the presence of the capacitor C_a. While at 5800 MHz, the electric-field distribution indicates that the corresponding resonant mode is a higher-order mode of the first slot. The results indicate that the inductor L_f and the capacitor C_a lead to the wide high band for the antenna to cover the 5.2-GHz and 5.8-GHz WLAN operation.

2.2. Parametric Study

By adjusting the inductor L_f and the capacitor C_a, the multiband operation of the antenna can be controlled. Figure 5 shows the simulated return loss as a function of the capacitor C_a for the proposed antenna, and other parameters are the same as shown in Figure 1. Results of the capacitor C_a varied from 0.6 to 1.6 pF are shown. When a smaller value of the C_a is selected (see the 0.6-pF curve in the figure), the resonant mode at higher frequencies cannot occur in the desired 5.2/5.8-GHz bands, and the resonant mode at lower frequencies is larger than 2.4 GHz. On the other hand, when a larger value of the C_a is selected (see the 1.6-pF curve), the resonant mode at higher frequencies can still cover the desired 5.2/5.8-GHz bands, and the resonant mode at lower frequencies is shifted to be lower than 2.4 GHz. The results indicate that the capacitor C_a is effective in obtaining the multiband operation of the antenna.

Figure 6 shows the simulated return loss for the inductor L_f varied from 1.0 to 2.0 nH. Other parameters are fixed as given in Figure 1. Results show that very small effects on the resonant mode at about 2.4 GHz are seen. On the other hand, there are some effects on the resonant modes at higher frequencies, especially the one at about 5.8 GHz. This again confirms that the inductor L_f mainly contributes to the resonant mode for covering the 5.8-GHz WLAN band.

Effects of the feedline position d on the antenna performance are also studied. Results of the simulated return loss for the position d varied from 2 to 4 mm are shown in Figure 7. Other parameters are the same as in Figure 1. In this case, large effects of the resonant mode at about 5.2 GHz are seen. This is largely because the tuning stub (section AA′) can cause relatively large effects on exciting the second slot (section BD). On the other hand, since the first slot has a larger length than the second slot, it is reasonable that the effects of the position d on the resonant modes at about 2.4 and 5.8 GHz contributed by the first slot are relatively small.

3. EXPERIMENTAL RESULTS

The proposed antenna shown in Figure 1 was fabricated and tested. The photos of the fabricated antenna, including the enlarged front and back views of the antenna, are shown in Figure 8. The measured and simulated return losses for the fabricated antenna are presented in Figure 9. Agreement between the measured data and simulated results is obtained. The impedance matching for frequencies in the 2.4/5.2/5.8-GHz WLAN bands is generally less than 10 dB. Figure 10 shows the measured and simulated antenna efficiencies for the fabricated antenna. Fair agreement between the measurement and simulation is also seen. The measured antenna efficiencies are about 64–82% in the 2.4-GHz band and better than 85% in the 5.2/5.8-GHz band. The obtained antenna efficiencies are acceptable for practical applications.

Figure 11 shows the measured and simulated radiation patterns for the fabricated antenna. Representative results at 2442 MHz for the low band and at 5500 MHz for the high band are shown. The measured patterns generally agree with the simulated patterns. At both frequencies, stronger radiation in the $+y$ direction than in the $-y$ direction is seen for the patterns in the $y-z$ and $x-y$ planes. This is reasonable since the antenna is disposed along the right-hand-side edge of the main circuit board. In the $x-z$ plane pattern, stronger radiation is also seen, especially at 2442 MHz. This is largely because the excited surface currents on the ground plane of the main circuit board may also contribute to the radiation. It is also noted that there are generally no null radiation in the radiation patterns for both frequencies. This radiation property is advantageous for the antenna to achieve better coverage in the practical applications.

4. CONCLUSION

An open-slot antenna with a narrow width of 1 mm to be promising for disposing along the narrow region between the display panel and metal frame of the modern smartphone has been proposed. In addition, the antenna requires a short length of 12.7 mm only, which is about 0.1 wavelength at 2.45 GHz, for covering the 2.4/5.2/5.8-GHz WLAN operation. The techniques of applying a capacitor across the narrow slot and an inductor in the microstrip feedline to achieve multiband operation for the antenna have been addressed. Good radiation characteristics for frequencies in the 2.4/5.2/5.8-GHz WLAN bands have also been obtained. The proposed antenna makes it promising to be employed within the narrow regions along the side edge of the modern metal-framed smartphone.

REFERENCES

1. R.J. Hill, R.W. Schlub, and R. Caballero, Antennas for handheld electronic devices with conducting bevels, U.S. Patent no. 7,924,231 B2, 2011.
2. C. Dong, B. Zhou, and C.L. Tang, Antenna structure for using a metal frame of a mobile phone, U.S. Patent no. 8,963,785 B2, 2015.
3. B. Yuan, Y. Cao, G. Wang, and B. Cui, Slot antenna for metal-rimmed mobile handset, IEEE Antennas Wireless Propag Lett 11 (2012), 1334–1337.
4. Y.L. Ban, Y.F. Qiang, Z. Chen, K. Kang, and J.H. Guo, A dual-loop antenna design for hepta-band WWAN/LTE metal-rimmed smartphone applications, IEEE Trans Antennas Propag 63 (2015), 48–58.
5. J.H. Ahn, Y.J. Kim, D.H. Kim, J.H. Lee, and S.H. Kim, Mobile terminal having metal case and antenna structure, U.S. Patent no. 8,054,231 B2, 2011.
6. K. L. Wong and Y. J. Li, Low-profile open-slot antenna with three branch slots for triple-wideband LTE operation in the metal-framed smartphone, Microwave Opt Technol Lett 57 (2015), 2231–2238.
7. K.L. Wong and C.Y. Tsai, Low-profile dual-wideband inverted-T open slot antenna for the LTE/WWAN tablet computer with a metallic frame, IEEE Trans Antennas Propag 63 (2015), 2879–2886.
8. K.L. Wong, H.J. Jiang, and Y.C. Kao, High-isolation 2.4/5.2/5.8 GHz WLAN MIMO antenna array for laptop computer application, Microwave Opt Technol Lett 55 (2013), 382–387.
9. T.W. Kang and K.L. Wong, Isolation improvement of 2.4/5.2/5.8 GHz WLAN internal laptop computer antennas using dual-band

strip resonator as a wavetrap, Microwave Opt Technol Lett 52 (2010), 58–64.
10. S.W. Su, High-gain dual-loop antennas for MIMO access points in the 2.4/5.2/5.8 GHz bands,IEEE Trans Antennas Propag 58 (2010), 2412–2419.
11. J.H. Yoon and Y.C. Lee, Modified bow-tie slot antenna for the 2.4/5.2/5.8 GHz WLAN bands with a rectangular tuning stub, Microwave Opt Technol Lett 53 (2011), 126–130.
12. K.L. Wong and P.R. Wu, Dual-wideband linear open slot antenna with two open ends for the LTE/WWAN smartphone, Microwave Opt Technol Lett 57 (2015), 1269–1274.
13. K.L. Wong and Z.G. Liao, Passive reconfigurable triple-wideband antenna for LTE tablet computer, IEEE Trans Antennas Propag 63 (2015), 901–908.
14. P. Bevelacqua, Dynamically adjustable antenna supporting multiple antenna modes, U.S. Patent no. 8,982,002 B2, 2015.
15. C.I. Lin and K.L. Wong, Printed monopole slot antenna for internal multiband mobile phone antenna, IEEE Trans Antennas Propag 55 (2007), 3690–3697.
16. K.L. Wong, P.W. Lin, and C.H. Chang, Simple printed monopole slot antenna for penta-band WWAN operation in the mobile handset, Microwave Opt Technol Lett 53 (2011), 1399–1404.

A SUSPENDED STRIPLINE BANDPASS FILTER USING HYBRID TRANSMISSION LINE STEPPED IMPEDANCE RESONATOR

ZhaoXu Xu, YiYao Hu, Yongpin P. Chen, Kai Kang, and Joshua Le Wei Li
Department of Electronic Engineering, University of Electronic Science and Technology of China, Chengdu 611731, China; Corresponding author: 329363599@qq.com

Received 4 August 2015

ABSTRACT: *In this article, a suspended stripline bandpass filter using hybrid transmission line stepped impedance resonator (HTLSIR) is proposed. SSL has been proven to be an excellent transmission-line system for realizing different types of filters. However, due to the effective permittivity being too close to unity, the size of the distributed elements is usually very large. The novel resonator introduced in this letter contains a section of hybrid transmission line which consists of the SSL and the microstrip line. The characteristics of the HTLSIR have been analyzed clearly. The novel SSL filter is designed, fabricated, and tested. Both simulated and measured results are presented.* © 2016 Wiley Periodicals, Inc. Microwave Opt Technol Lett 58:892–895, 2016; View this article online at wileyonlinelibrary.com. DOI 10.1002/mop.29697

Key words: *suspended stripline; hybrid transmission line stepped impedance resonator (HTLSIR); bandpass filter; resonant frequency; unloaded quality factor*

1. INTRODUCTION

In modern microwave communication systems, bandpass filter is an essential component, which is usually used in both receivers and transmitters. With the rapid development of modern communication systems, bandpass filters play more important roles in a variety of microwave circuits. The development of bandpass filters has been focused on compact size and high performance.

Due to the excellent performance of the different types of SSL filters [1–8], SSL has proven to be an excellent transmission-line system. Compared to other planar transmission lines, such as coplanar waveguide, microstrip line, the SSL has a bigger cross-section, which means that it has lower dielectric loss and lower current densities. Hence, SSL resonators have higher unloaded quality factor resulting in lower loss. Moreover, utilizing both sides of the relatively thin substrate offers an increased flexibility in circuit design, which is not as easily available in other types of planar lines. In recent years, the SSL bandpass filters have become popular in communication systems due to their advantages of ease in manufacture, low cost, and high practicality.

The miniaturization is always a very important requirement to any types of filters. The resonator introduced in Ref. 2 is small in general, but is still big for applications in the lower band of radio frequencies. In Ref. 4, a novel resonator with cuboid-shaped bricks of metal are incorporated into the SSL channel in the vicinity of the open-circuited side to enhance the capacitive loading. The performance is achieved by changing the metal channel of the conventional SSL filter, so it will increase the complexity of processing the channel. The resonator proposed in this letter, however, does not need to change the channel, and can be easily realized by printed circuit technology. Furthermore, the new design provides more capacitive loading than the resonator in Ref. 2. However, it will also decrease the unloaded quality factor of the resonator. In other words, the insertion loss will be increased slightly.

Finally, a novel fifth order SSL bandpass filter is designed, produced, and measured to verify the high performance of the novel resonator. The SSL filter proposed in this article has been fabricated on a RO 4003 substrate, with a thickness of 0.254 mm and dielectric constant of 3.55. It is shown that the new resonator can be used in SSL filter to effectively reduce the size of filter.

2. HYBRID TRANSMISSION LINE STEPPED IMPEDANCE RESONATOR

In order to show the different characteristics among the three types of resonators, the schematic diagrams are shown in Figure 1. The top view of a conventional quasi-lumped SSL resonator, which is equivalent to a parallel LC-circuit, is shown in Figure 1(a). The resonator introduced by Ruf and Menzel [4] is shown in Figure 1(b). There is a metal brick on the back of the resonator with a gap of 1 mm to the substrate. The capacitive loading can be enhanced so that the resonant frequency can be decreased while keeping the size of the resonator unchanged. The novel resonator proposed in this letter has a part of metallization at its back side, which can be regarded as a microstrip line. Therefore, the novel resonator has two advantages. First, when the three types of resonators have the same size, the resonant frequency of the new design in this letter is the lowest. Secondly, the resonator does not need to change the channel of SSL filter to enhance the capacitive loading, so it is very convenient for fabrication. The resonant frequency of type II resonator can be modified by changing the length of the brick. On the other hand, the resonant frequency of type III resonator can be altered just by changing the length of the back-side metal. Moreover, the adjusting range of resonant frequency of type III resonator is much broader than the type II resonator.

If there was no gap between the metal brick and the substrate in type II resonator, it would become the type III resonator. However, the unloaded quality factor of the type II resonator is lower than type III resonator, because the metal brick reduces the size of the whole channel.

The stepped impedance resonator is extensively studied in Ref. 8. We can analyze the novel resonator in a similar way. Figure 2 shows the fundamental element of HTLSIR which can be divided into several parts, including an open-end, a short-end, an impedance step, and a section of hybrid transmission line. Characteristic impedance and corresponding electrical length of the transmission lines between the open and short-circuited ends are defined as Z_1,